Journal of Geodetic Science

• 1(1) • 2011 • 59-73 DOI: 10.2478/v10156-010-0008-1 •

Comprhensive Approach to the Analysis of the 3D Kinematics Deformation with appliction to the Kenai Peninsula

Research Article

M. Mashhadi Hossainali[1*], M. Becker[2†], E. Groten[2‡]

1 K.N.Toosi University of Technology, Faculty of Geodesy and Geomatics Engineering, 1346 Valiasr Street, Mirdaamaad intersection, Tehran, Iran
2 Technical University of Darmstadt, Institute of Physical Geodesy, Petersenstrasse 13, Darmstadt, Germany

Abstract:

The problem of analyzing surface deformation of the Earth's crust in three-dimensions is discussed. The isoparametric and Lagrangian formulations of deformation are extended from 2D to 3D. Analytical and numerical investigation of problem conditioning proves that analyzing the 3D kinematics of deformation can be an ill-posed problem. The required mathematical elements for solving this problem, including sensitivity analysis of the deformation tensor and regularization, are proposed. Regularized deformation tensors were computed using the method of truncated singular value decomposition (TSVD). The optimal regularization parameter was attained by minimizing regularization errors. Regularization errors were assessed using the corresponding 2D results of deformation analysis. The proposed methods were applied to the GPS network in the Kenai Peninsula, south-central Alaska, in order to compute the 3D pattern of postseismic crustal deformation in this area. Computed deformation in the vertical direction is compared to the existing pattern of vertical deformation obtained from the combination of precise leveling, gravity and GPS measurements from other studies on this area.

Keywords:

Deformation analysis • sensitivity analysis • principal component analysis • regularization • truncated singular value decomposition (TSVD) • GPS deformation

Received 21 November 2010; accepted 29 November 2010

1. Introduction

According to Berber et al. (2003), the earliest known publication on the application of geodetic techniques to the analysis of the deformation of the Earth's surface is Terada and Miyabe (1929). They use strain analysis for describing seismic surface deformation. Since then, repeated geodetic observations have been used to derive displacement fields and to analyze geodynamical phenomena. A variety of methods have been developed and proposed. Characteristic features of the geometric geodetic analysis of deformation have also been explored (Frank 1966; Welsch 1979; Bibby 1982; Chen 1991; Altiner 1999; Krumm and Grafarend 2002, Dermanis and Grafarend, 1981; Xu, 1995, 1997; Xu et al., 2000).

For geodetic networks without a connection to an external reference frame, free network adjustment are widely used to derive deformation parameters. It is now commonly accepted that absolute displacements cannot be uniquely determined unless the geodetic network is tied to an external reference frame (Segall and Matthews, 1988; Xu, 1997; Xu et al., 2000). The invariance of strain parameters have also been thoroughly analyzed (Dermanis, 1981, 1985; Dermanis and Grafarend, 1992; Grafarend, 1992; Biby, 1982; Lambeck, 1988 and Xu, 1994, 1995, 2000). It is also commonly accepted that components of the strain tensor are not all invariant and therefore cannot be uniquely determined. Xu et al., (2000) mathematically investigated the invariance of the deformation

*E-mail: hossainali@kntu.ac.ir
†E-mail: becker@ipg.tu-darmstadt.de
‡E-mail: groten@ipg.tu-darmstadt.de

tensor elements and derived quantities such as principal and shear strains.

Assuming that small vertical deformations have a negligible effect on the horizontal ones (Lichtenegger and Sünkel 1989), the majority of existing geodetic techniques systematically ignore the effect of vertical deformations on the horizontal ones. However, deformation of the Earth's crust is a 3D phenomenon. Therefore, the formulation and study of deformation in 3D is necessary to properly account for the cross-correlation of the vertical and horizontal deformations.

Mathematically, deformation can be defined as the mapping that transforms a body from its unstrained to deformed state. This can be written as:

$$x_2 = f(\Theta, x_1) \tag{1}$$

where, x_1 and x_2 are $3p \times 1$ vectors whose elements are the coordinates of the material points of deformable body before and after deformation. The vector-valued function f is the corresponding mapping function and p is the number of the points that have been considered in the problem. Deformation of the body is characterized through the mapping function f and deformation parameters Θ.

This approach to the analysis of deformation defines the mathematical basis in the theory of shape analysis (Dryden and Mardia 1998; Crosilla 2003). For example, thin-plate spline functions are commonly used as the mapping function for characterizing the deformation. It is not possible to establish constitutive equations within the context of continuum mechanics (e.g. Flügge 1972) using parameters that describe the deformation of a body by means of theory of shape analysis. Therefore, they are not tailored to the modeling of the dynamics of deformation.

When the mapping function f in Eq. (1) is taken as an affine transformation, deformation parameters benefit from direct physical implications: they characterize homogeneous deformation of a deformable body (Sokolnikoff 1956). Moreover, the mapping function can be written as the sum of a symmetric matrix (strain tensor) and a skew-symmetric matrix (rigid body rotations). Based on this idea, Brunner (1979) proposed a 3D approach for the analysis of the overall deformations of the Earth's crust.

Wittenburg (2003) studied the problem of 3D analysis of deformation and argued that, due to the deficit of required information, a 3D description of deformation based on geodetic surveys is not possible. This argument is not generally correct because depending on the methodology used in the analysis of deformation, the 3D description of deformation may be possible. For example, the theory of analytical surface deformation analysis (Altiner 1999) takes into account the 3D nature of deformation through the computation of the so-called external measures of deformation. However, it is not possible to establish a functional relationship between the external measures of deformation (such as the parameters that characterize the deformation) and stress (i.e. constitutive equations) for all types of rheologies. In addition, the interpretation of the external measures of deformation is difficult.

In this paper, the application of two new approaches for 3D analyses of deformation of the Earth's surface is given. By analyzing the conditioning of the problem, both analytically and numerically, it is shown that the problem of the 3D kinematics of deformation can be an ill-posed problem. Truncated Singular Value Decomposition is used to regularize the problem and obtain a three-dimensional pattern of deformation for the test area presented here. Regularization errors have been assessed using the corresponding two dimensional results of deformation analysis. The computed pattern of vertical deformation is compared to the existing pattern of vertical deformation in the test area of this research. The conformance of the obtained pattern of deformation to the previously obtained results proves that estimated parameters of deformation are not dominated by regularization errors.

2. Test Area

2.1. Dominant factors contributing to the deformation of the test area

Southern Alaska, including the Aleutian Island chain (extending from Fairbanks in the north to the Gulf of Alaska in the south) is one of the world's most active seismic zones. This area is a part of a vast seismic zone known as Circum-Pacific seismic belt that coincides with the world's largest orogenic belt and contains most of the Earth's active volcanoes. Seismicity along the Circum-Pacific belt, and south-central Alaska, is driven by the anticlockwise motion of the Pacific Plate. This results in subduction in the north (Alaska) and west (Japan to New Zealand).

South central Alaska was severely affected by the 1964 PWS (Prince William Sound) earthquake. Kanamori (1977) estimated a moment magnitude of $M_w = 9.2$ for this earthquake. The main shock was reportedly felt throughout most parts of Alaska, 600 miles to 800 miles from the epicenter (Hansen and Eckel 1966). The epicenter of this earthquake is shown in Figure 1. Based on triangulation data prior to this earthquake and post earthquake measurements in 1964 and 1965, Parkin (1972) estimated horizontal displacements of 15 m at Seward (SE) with respect to the station Fishhook (FI) shown in Figure 1.

Estimates of coseismic horizontal displacements exceed 20 m in some parts of the affected area (Parkin, 1972). During this event, most of the Kenai Peninsula subsided coseismically. In contrast, the area east (the oceanic crust) underwent a coseismic uplift. Coseismic uplift exceeded 12 m on Montague Islands (Figure 1) -- (Plafker 1971). Plafker (1971) reported a maximum coseismic subsidence of 2 m in subsided area. Maximum coseismic subsidence occurred on the southeast portion of Kodiak Island, along the east-central region of the Kenai Peninsula and at the eastern end of Turnagain Arm (Figure 1). The most profound effects of this event were seen in south-central Alaska, in the cities of Anchorage, Valdez, Cordova and on Kodiak Island, southwest of the Kenai Peninsula (Figure 1). Similar displacements were also observed by Holdahl and Sauber (1994).

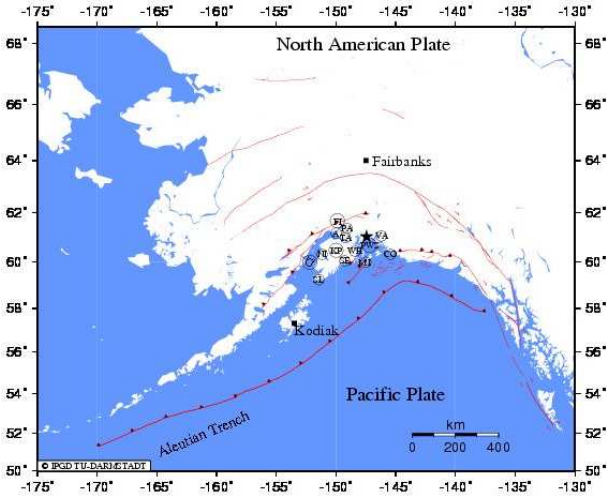

Figure 1. The southern Alaska active faults. KP: Kenai Peninsula, PWS: Prince William Sounds, CI: Cook Inlet, TA: Turnagain Arm of Cook Inlet, A: Anchorage, NI: Nikishki, SL: Seldovia, SE: Seward, WH: Whitter, CO: Cordova, VA: Valdez, FI: Fishhook, PA: Palmer. Star shows the epicenter of the 1964 Alaskan Earthquake.

2.2. Postseismic Deformation

Postseismic uplift in the Kenai Peninsula was firstly reported by Brown et al. (1977), based on tidal observations at Anchorage and four geodetic leveling surveys between Whittier and Anchorage. They reported a maximum uplift of 0.55 m at a location midway between the two cities. Brown et al. (1977) suspected that the observed uplift followed an elongate pattern. They found evidence of domical pattern for the postseismic uplift in this area.

Savage and Plafker (1991) updated the Brown et al., (1997) study by analyzing tide-gage records in Seward, Seldovia and Nikishka. They also observed postseismic uplift at locations where coseismic subsidence had occurred and postseismic subsidence at locations where coseismic uplift had occurred. Cohen and Freymueller (1997) also confirmed the domical pattern of postseismic deformation within the Kenai Peninsula.

GPS measurements supplement the suite of geodetic measurements scientists use to improve their understanding of the mechanisms that control ongoing crustal deformation in this area. Cohen et al. (1995) reported on the combined use of GPS results, gravity measurements and leveling results of the 1964 survey. They reoccupied six of the 1964 leveling benchmarks on the Kenai Peninsula between Seward and Nikishka using geodetic GPS receivers. Using gravity measurements, a high-resolution local geoid was computed. Geodetic heights were estimated, transformed to orthometric heights using the geoid model and then compared to the leveling results. Since orthometric heights of only one epoch were based on the computed geoid model, the detected deformations were caused by errors in the geoid. This study provided insight into the cumulative 1964-1993 postseismic vertical deformations in this area. Based on their analysis, a maximum uplift of 0.90 m to 1.1 m was observed in the middle of the peninsula. Cohen et al. (1995) suggested that a broad arch of postseismic uplift extending at least from Kodiak Island to northeast of Anchorage was ongoing in this area.

Cohen and Freymueller (1997) combined the results of the leveling survey immediately after the Prince William Sound earthquake of 1964 and the GPS results from 1993 and 1995. They used NGS geoid height model GEOID96 for transforming the GPS ellipsoidal to orthometric heights. In their analysis they proposed an elongate domical pattern for the postseismic uplift in the Kenai region (Figure 2). They argued that the elongate dome is approximately 125 km wide with its major axis orienting southwest-northeast, following the trend of major tectonic features of this area. They estimated maximum uplift of about 0.90 m near the center of peninsula with an average rate as high as 30 mm/yr. This study presented the first detailed analysis of the spatial distribution of cumulative uplift over 30 years.

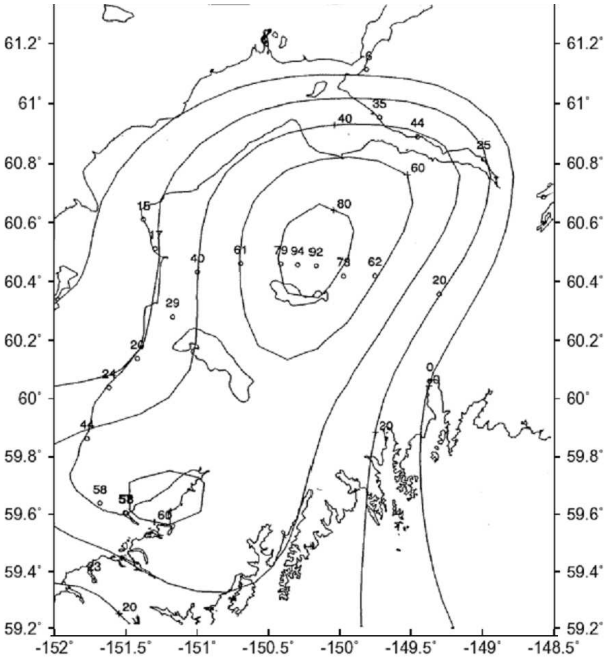

Figure 2. Domical pattern of vertical deformation computed using tidal, gravity and leveling observations, reproduced from Cohen and Freymueller (1997).

3. Methodology

Continuous deformation of a deformable body at a point can be either formulated in terms of the relative change between the distances of points from their surrounding points (isoparametric representation of deformation) or in terms of the change in their rel-

ative positions (Lagrangian representation of deformation) (Love 1944; Jaeger 1969). The basic assumptions in both approaches are that the points that contribute to estimating the parameters of deformation at one point (here are called contribution points) should fall within a small vicinity of the point at which the deformation parameters can be estimated (computation point) and that, deformation of the body is homogeneous.

Both approaches mentioned above have been used for estimating the 2D second rank deformation tensor e in the desired (ellipsoidal or spherical) coordinate system (e.g. Chen 1991; Altiner 1999). Elements of this tensor read as:

$$e_{xx} = \frac{\partial u}{\partial x}, e_{yy} = \frac{\partial v}{\partial y}, \quad e_{xy} = \frac{\partial u}{\partial y} + \frac{\partial v}{\partial x} \tag{2}$$

In these equations u and v are the deformation vector components in the x and y directions.

In this study, the mathematical formulation of the problem in isoparametric and Lagrangian representations of deformation are extended from 2D to 3D. For practical applications, the traditional least-squares technique may not be an appropriate mathematical tool due to variations in network size, network configuration and topography of the area.

Analyzing the coefficient or design matrix in the 3D Isoparametric and 3D Lagrangian representations of deformation provides an immediate insight into the practical aspects of this problem. To clarify this argument the analytical form of the design matrix in both isoparametric and Lagrangian formulations of the problem is given in a local rectilinear Cartesian coordinate system. In a local ENU-coordinate system these matrices read (see Hossainali, 2006 for further details):

$$A = \begin{bmatrix} \frac{\Delta E_{k1}^2}{L_{k1}^2} & \frac{\Delta N_{k1}^2}{L_{k1}^2} & \frac{\Delta E_{k1}\Delta N_{k1}}{L_{k1}^2} & \frac{\Delta E_{k1}\Delta U_{k1}}{L_{k1}^2} & \frac{\Delta N_{k1}\Delta U_{k1}}{L_{k1}^2} & \frac{\Delta U_{k1}^2}{L_{k1}^2} \\ \frac{\Delta E_{k2}^2}{L_{k2}^2} & \frac{\Delta N_{k2}^2}{L_{k2}^2} & \frac{\Delta E_{k2}\Delta N_{k2}}{L_{k2}^2} & \frac{\Delta E_{k2}\Delta U_{k2}}{L_{k2}^2} & \frac{\Delta N_{k2}\Delta U_{k2}}{L_{k2}^2} & \frac{\Delta U_{k2}^2}{L_{k2}^2} \\ \dots & \dots & \dots & \dots & \dots & \dots \\ \frac{\Delta E_{kp}^2}{L_{kp}^2} & \frac{\Delta N_{kp}^2}{L_{kp}^2} & \frac{\Delta E_{kp}\Delta N_{kp}}{L_{kp}^2} & \frac{\Delta E_{kp}\Delta U_{kp}}{L_{kp}^2} & \frac{\Delta N_{kp}\Delta U_{kp}}{L_{kp}^2} & \frac{\Delta U_{kp}^2}{L_{kp}^2} \end{bmatrix}_{p\times 6} \tag{3}$$

$$A = \begin{bmatrix} \Delta E_{k1} & 0 & \frac{1}{2}\Delta N_{k1} & 0 & \frac{1}{2}\Delta U_{k1} & 0 & 0 & \Delta U_{k1} & -\frac{1}{2}\Delta N_{k1} \\ 0 & \Delta N_{k1} & \frac{1}{2}\Delta E_{k1} & 0 & 0 & \frac{1}{2}\Delta U_{k1} & -\Delta U_{k1} & 0 & -\Delta E_{k1} \\ 0 & 0 & 0 & \Delta U_{k1} & \frac{1}{2}\Delta E_{k1} & \frac{1}{2}\Delta N_{k1} & \Delta N_{k1} & -\Delta E_{k1} & 0 \\ \dots & \dots & \dots & \dots & \dots & \dots & \dots & \dots & \dots \\ \Delta E_{kp} & 0 & \frac{1}{2}\Delta N_{kp} & 0 & \frac{1}{2}\Delta U_{kp} & 0 & 0 & \Delta U_{kp} & -\frac{1}{2}\Delta N_{kp} \\ 0 & \Delta N_{kp} & \frac{1}{2}\Delta E_{kp} & 0 & 0 & \frac{1}{2}\Delta U_{kp} & -\Delta U_{kp} & 0 & -\Delta E_{kp} \\ 0 & 0 & 0 & \Delta U_{kp} & \frac{1}{2}\Delta E_{kp} & \frac{1}{2}\Delta N_{kp} & \Delta N_{kp} & -\Delta E_{kp} & 0 \end{bmatrix}_{3p\times 9} \tag{4}$$

where ΔE_{ki}, ΔN_{ki} and ΔU_{ki} $(i = 1, 2, \dots, p)$ are the components of the relative position vector $\overrightarrow{ki}$, between computation point k and contribution points i, in the local coordinate system and L_{ki} is the length of this vector.

For example, it can be seen that if either of the baseline components are zero (e.g. no height differences between the network stations) matrix A would not be of full column rank. When this condition is approximately fulfilled, which is common in practice, some of the columns of the design matrix (columns 4, 5 and 6 in the isoparametric approach and column 5 in the Lagrangian approach) will approach zero. Consequently, the condition number of the system of normal equations is much larger than one and the problem is an ill-conditioned problem. Therefore, the least-squares technique is not an adequate mathematical tool for solving the problem.

3.1. Elements of the 3D analysis of Deformation

Mathematical problems that can be solved numerically are classified as well-posed and ill-posed. A problem is considered well-posed if its solution exists, is unique and continuous under infinitesimal changes of inputs. A problem is ill-posed if any of these conditions is violated (Tikhonov and Arsenin 1977). Perturbation theory and regularization techniques are standard mathematical tools for treating discrete ill-posed problems.

The analysis of the effects of all possible perturbations (observational and computational errors) on estimated parameters compared to the exact solution is the main aim of perturbation theory (Dief 1986). The following theorems within this theory elaborate the concept of condition number and its impact on the sought solution of a system of simultaneous equations. Consider the linear system of equations:

$$\begin{aligned} &Ax = b, \text{ where: } A \in R^{n\times m}, x \in R^{m\times 1} \\ &\text{And } b \in R^{n\times 1} \text{ and n} \geqslant m \end{aligned} \tag{5}$$

In a consistent system of simultaneous equations $A \in R^{n\times n}$ and is nonsingular, what will be the effect on the solution x if we apply small perturbations ΔA and Δb to A and b respectively:

Theorem 1: Let A be nonsingular and consider the consistent linear system $Ax = b$. The upper bound limit for the error in

the exact solution x due to perturbations ΔA and Δb of A and b respectively in the perturbed linear system $(A + \Delta A)\,\tilde{x} = b + \Delta b$, where $\tilde{x}$ is the vector of perturbed unknown parameters, is:

$$\frac{\|\tilde{x} - x\|}{\|x\|} \leqslant \frac{k_2(A)}{\left(1 - \|A^{-1}\Delta A\|\right)}\left[\frac{\|\Delta b\|}{\|b\|} + \frac{\|\Delta A\|}{\|A\|}\right] \qquad (6)$$

where $k_2(A) = \|A\|_2 \quad \|A^{-1}\|_2$ is called the condition number of A (Jain et al. 2003).

Corollary 1: Let A be a nonsingular and square matrix in the linear system $Ax = b$. The upper bound limit for the error in the exact solution x due to perturbation Δb in the perturbed linear system $A\tilde{x} = b + \Delta b$ is:

$$\frac{\|\tilde{x} - x\|}{\|x\|} \leqslant k_2(A)\frac{\|\Delta b\|}{\|b\|} \qquad (7)$$

This is immediately followed from Theorem 1, $\Delta A = O$ where O is an n-by-n null matrix.

Inequality Eq. 7 shows that in a system of linear equations, the condition number acts as a noise amplifier. In other words, the solution is not continuous under infinitesimal changes of inputs when $k_2(A)$ is large. The system of equations $Ax = b$ is said to be ill-conditioned if $k_2(A)$ is large.

Similar to the linear system (Eqs. 6 and 7), the sensitivity of a least-squares solution can also be analyzed. The following theorem provides a norm-wise upper bound limit for the sensitivity of least-squares solution based on the perturbations ΔA and Δb of the input parameters A and b.

Theorem 2: Let $A \in R^{m\times n}\,(m \geqslant n)$ and $A + \Delta A$are both of full rank; and let: $\|b - Ax\|_2 = \min, r = b - Ax$; $\|(b + \Delta b) - (A + \Delta A)\,\tilde{x}\| = \min, s = b + \Delta b - (A + \Delta A)\,\tilde{x}$; $\|\Delta A\|_2 \leqslant \varepsilon\|A\|_2, \quad \|\Delta b\|_2 \leqslant \varepsilon\|b\|_2$, then provided that $k_2(A)\varepsilon < 1$ (Higham 2002):

$$\frac{\|x - \tilde{x}\|}{\|x\|} \leqslant \frac{k_2(A)\varepsilon}{1 - k_2(A)\varepsilon}\left(2 + (k_2(A) + 1)\frac{\|r\|_2}{\|A\|_2\,\|x\|_2}\right) \qquad (8)$$

Corollary 2: Sensitivity of least-squares solutions is measured by $k_2(A)$ when the residuals are small or zero and by $k_2(A)^2$ otherwise. Equations (3) and (4) show that ill-conditioning is a property of the system of equations (it only depends on the design matrix A of this problem) and not a property of the adopted numerical algorithm for solving the problem. Therefore, ill-conditioning cannot be simply treated by using a better numerical algorithm. Instead, a better-conditioned system should be sought to replace the ill-conditioned problem (e.g. Aster et al. 2005). The new system might be based on a reformulation of the problem or its replacement by a stable one which is literally based on the original system. In inversion theory, the latter is normally termed as regularized system.

First, the instability of least-squares solution is analyzed. The instability of the least-squares solution in both the 3D Isoparametric and 3D Lagrangian representations of deformation are analyzed using the discrete Picard condition (Hansen 1990). By regularizing a problem, its sensitivity to the input perturbations is reduced. However, this comes at the cost of introducing artifacts into the solution. Therefore, a tradeoff between the resolution and sensitivity of the system should be sought. This is the well-known tradeoff between stability and resolution. It is also customary to look for an optimum regularization parameter.

Among different regularization techniques, Truncated Singular Value Decomposition or TSVD (Hansen, 1990 and Xu, 1998) is used for regularizing the problem of the 3D representation of deformation of the Earth's crust due to its simplicity in application and visualization of the process.

The flow-diagram of Figure 3 outlines the mathematical steps for solving the problem of analyzing deformation of the Earth's crust in three dimensions. The different elements of this process are discussed in the following sections of this paper.

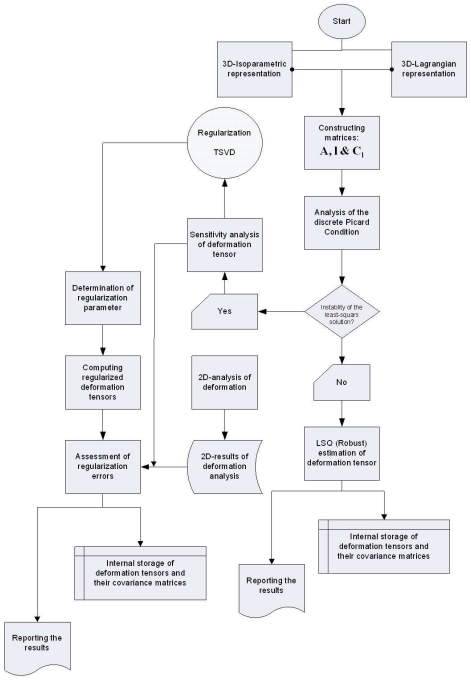

Figure 3. Elements of the 3Dkinematic approach to the analysis of the Earth's surface deformations.

3.1.1. Discrete Picard Condition

If x_t and x_k are exact and regularized solutions of the discrete ill-posed problem:

$$\min_x \|Ax - b\|_2, \; A \in R^{m\times n}, \; m \geqslant n \tag{9}$$

where $\|x_t - x_k\|_2$ is a measure for regularization error. When TSVD is used for regularizing the problem, an upper bound limit for the regularization error is given by (Hansen 1990):

$$\|x_t - x_k\|_2 \leqslant p^{\frac{1}{2}} \max_{1\leqslant i\leqslant p-k} \left\{ \frac{|U_{.,i}^T b|}{\sigma_i} \right\} \tag{10}$$

where σ_i, $i = 1, 2, .., p, p+1, ..., k$, are the singular values, vectors $U_{.,i}$are the corresponding left singular vectors in the spectral representation of matrix A and k is the total number of singular values with p nonzero values. Products: $|U_{.,i}^T b|$ are normally called Fourier coefficients.

Inequality Eq. (10) shows that smaller regularization error is expected to be present in the regularized solution, if, on average, the Fourier coefficients decay faster than the corresponding singular values. This property is known as the discrete Picard condition. The condition is numerically analyzed using the moving geometric mean where $q < n - 2$ is an integer.

$$\rho_i = \frac{\prod_{j=i-q}^{i+q} |U_{.,i}^T b|}{\sigma_i}, \; i = q+1, ..., n-q \tag{11}$$

Spectral representation of the least-squares solution establishes a close connection between the instability of this solution and the Picard condition. This interrelation can also be seen in Ineq. (10) by settings $k = 0$. To clarify this argument, the least-squares solution of Eq. (9) has to be expressed in its spectral form. According to the geometric SVD theorem (see theorem 4), matrix A in the least-squares problem Eq. (9) can be expressed as the product of orthonormal matrices $U = [U_{.,1}, U_{.,2}, ..., U_{.,m}] \in R^{m\times m}$, $V = [V_{.,1}, V_{.,2}, ..., V_{.,n}] \in R^{n\times n}$ and the diagonal matrix $\Sigma = diag(\sigma_1, \sigma_2, ..., \sigma_n) \in R^{m\times n}$, where $\sigma_1 \geqslant \sigma_2 \geqslant ... \geqslant \sigma_p \geqslant \sigma_{p+1} = ... = \sigma_n = 0$, that is:

$$A = U\Sigma V^T \tag{12}$$

Substituting this expression in the maximum likelihood solution $x = \left(A^T A\right)^{-1} A^T b$ gives:

$$x = \left(V^T\right)^{-1} \Sigma^{-1} \left(\Sigma^T\right)^{-1} V^{-1} V \Sigma^T U^T b = \left(V^T\right)^{-1} \Sigma^{-1} U^T b \tag{13}$$

For the p non-zero singular values, Eq. (13) takes the following form:

$$x = V \left[\frac{1}{\sigma_1} U_{.,1}^T b \;\; \frac{1}{\sigma_2} U_{.,2}^T b \;\; ... \;\; \frac{1}{\sigma_p} U_{.,p}^T b \right]^T \tag{14}$$

In the presence of random noise, even if the true data were orthogonal to $U_{.,i}$s, $U_{.,i}^T b$ is very likely to be non-zero. When these non-zero values are divided by small singular values and then multiplied by $V_{.,i}$, an unstable solution is obtained. Therefore, according to Eq. (14) for a stable least-squares solution, the discrete Picard condition is automatically fulfilled. In other words, the discrete Picard condition is also a necessary condition to obtain a stable least-squares solution. When the condition is not fulfilled, the instability of least-squares solution is automatically assured. Figure 4 shows the Picard condition for two stations KEN1 and C85G of the GPS network in Kenai. The condition is not fulfilled at both of these stations. Therefore, the least-squares solution will be sensitive to observational and computational errors.

3.1.2. Sensitivity Analysis of the Deformation Tensor

Within the sensitivity analysis of the deformation tensor, the instability of the parameters of deformation is analyzed. The sensitivity of these parameters to the network configuration and input errors is analyzed. Since the problem of the 3D representation of deformation is an ill-posed problem, we are no longer concerned with the multivariate confidence regions, commonly reported in the sensitivity and precision analysis of geodetic networks. Moreover, because the sensitivities of all of the parameters to the perturbation of inputs are of equal interest, another mathematical technique is required. We show that principal component analysis (PCA) is an appropriate mathematical tool for this purpose. To clarify this argument, the theoretical back ground of PCA is firstly re-established through the following theorems.

Consider a vector of random variables $x = [x_1, x_2, ..., x_p]^T$ with the covariance matrix Σ. According to the propagation law of errors, any two linear combinations y_h and y_k of the random variables $x_1, x_2, ..., x_p$; i.e.: $y_h = \sum_{i=1}^{p} l_{ih} x_i$ and $y_k = \sum_{i=1}^{p} l_{ik} x_i$ have the variance $Var(y_n) = l_n^T \Sigma l_n, n = h$ or k, and the covariance $Cov(y_k, y_h) = l_h^T \Sigma l_k$. By definition, principal components are uncorrelated linear combinations $y_1, y_2, ..., y_p$whose variances are as large as possible. Such uncorrelated linear combinations can be established through the following theorem:

Theorem 3: Consider the positive definite matrix Σ whose spectral decomposition is given by the eigenvalue-eigenvector pairs (λ_i, e_i), $i = 1, ..., p$, in which $\lambda_1 \geq \lambda_2 \geq ... \geq \lambda_p \geq 0$ is assumed. Then $\max_{z\neq 0} \frac{z^T \Sigma z}{z^T z} = \lambda_1$ is attained when $z = e_1$ and $\max_{z \perp e_1,...,e_k} \frac{z^T \Sigma z}{z^T z} = \lambda_{k+1}$ is attained when $z = e_{k+1}$, $k = 1, 2, ..., p-1$(Johnson and Wichern 2002).

Corollary 3: Let Σ be the covariance matrix associated with the random vector $x = [x_1, x_2, ...,x_p]^T$. Let Σ have the spectral decomposition $(\lambda_1, e_1), (\lambda_2, e_2)\tilde{}\left(\lambda_p, e_p\right)$ where for the singular values λ_i: $\lambda_1 \geq \lambda_2 \geq ... \geq \lambda_p \geq 0$ is assumed and $e_h = [e_{1h}, e_{2h}, ..., e_{ph}]^T$ denote orthonormal singular vectors in its spectral form. The h^{th} principal component is then given by:

$$y_h = e_h^T x = e_{1h} x_1 + e_{2h} x_2 + ... + e_{ph} x_p \tag{15}$$

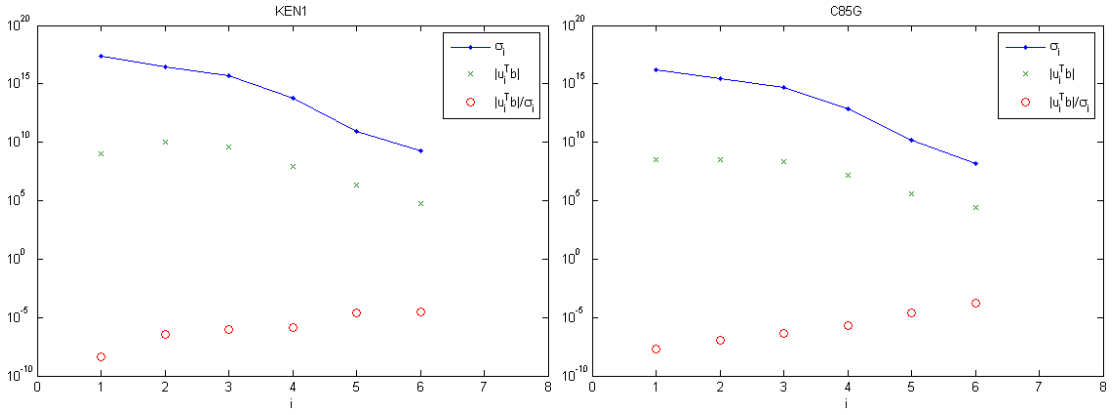

Figure 4. Discrete Picard Condition for two stations KEN1 (a) and C85G (b).

where for $h = 1, 2, ..., p$

$$Var\,(y_h) = e_h^T \Sigma e_h = \lambda_h \tag{16}$$

$$Cov\,(y_k, y_h) = e_h^T \Sigma e_k = 0, \text{ when } h \neq k \tag{17}$$

Corollary 4: If $y_h = \sum_{i=1}^{p} e_{ih} x_i$, $h = 1, 2, ..., p$, are the principal components of the positive definite matrix Σ, then the correlation coefficients of variables x_j and the principal components y_h are given by (Johnson and Wichern 2002):

$$Cor\,(x_j, y_h) = \frac{e_{jh}\sqrt{\lambda_h}}{\sigma_j},\ j, h = 1, 2, ..., p \tag{18}$$

The analysis of these correlation coefficients can identify the parameters that are equally correlated with the total variance λ_h of the h^{th} principal component.

To analyze the sensitivity of the deformation tensor, principal components of the normal matrix are set up. When the normal matrix is ill-conditioned, the computation of the covariance matrix is problematic. From a theoretical point of view, PCA can be applied to any positive definite matrix N (Johnson and Wichern 2002). This prerequisite is also a characteristic feature of the normal matrix in all geodetic problems. For this purpose, the normal matrix is firstly expressed in its spectral form.

The stability of the system can be visualized through the spectral representation of the normal matrix. Using Eq. (15) the corresponding principal components are then established. Each principal component organizes random variables (deformation parameters) into separate groups. The correlation coefficients between the principal components and all unknown parameters are then estimated using Eq. (18). Finally, the computed correlation coefficients are used for organizing the random variables of each group according to their individual correlation with the corresponding spectral value in ascending order. For smaller singular values, random variables that have larger correlation coefficients associated with the corresponding principal components are highly sensitive to perturbation of the input parameters. Figure 5 illustrates the results of the sensitivity analysis of the deformation tensor in one of the GPS stations in the crustal deformation array of the Kenai Peninsula.

3.1.3. Numerical Treatment of the 3D Representation of Deformation

The application of TSVD for solving linear discrete ill-posed problems like in Eq. (9) can be traced back to Hanson (1971) and Varah (1973). Later, Hansen (1987) analyzed the problem and compared it with Tikhonov (1963) and Philip (1962) regularization techniques. This study demonstrated that the TSVD is a favorable alternative for the standard Tikhonov-Philips regularization.

TSVD is based on the geometric SVD theorem:

Theorem 4: Let $A \in R^{n\times m}$ be a nonzero matrix with rank r. Then, there exist real numbers $\sigma_1 \geqslant \sigma_2 \geqslant ... \geqslant \sigma_r > 0$, an orthonormal basis $\{v_1, v_2, ..., v_m\}$ that spans R^m and an orthonormal basis $\{u_1, u_2, ..., u_n\}$ that spans R^n such that:

$$\begin{aligned} Av_i &= \begin{cases} \sigma_i u_i, 1 \leqslant i \leqslant r \\ 0, r+1 \leqslant i \leqslant m \end{cases} \\ A^T u_i &= \begin{cases} \sigma_i v_i, 1 \leqslant i \leqslant r \\ 0, r+1 \leqslant i \leqslant m \end{cases} \end{aligned} \tag{19}$$

Base vectors $\{u_1, u_2, ..., u_n\}$ and $\{v_1, v_2, ..., v_m\}$ are called the left and the right singular vectors respectively (Watkins 2002).

This study considers a system of normal equations $r = rank(A) = n$ (rank of A is full) and there is no zero spectral value in the spectral decomposition of the normal matrix. Instead,

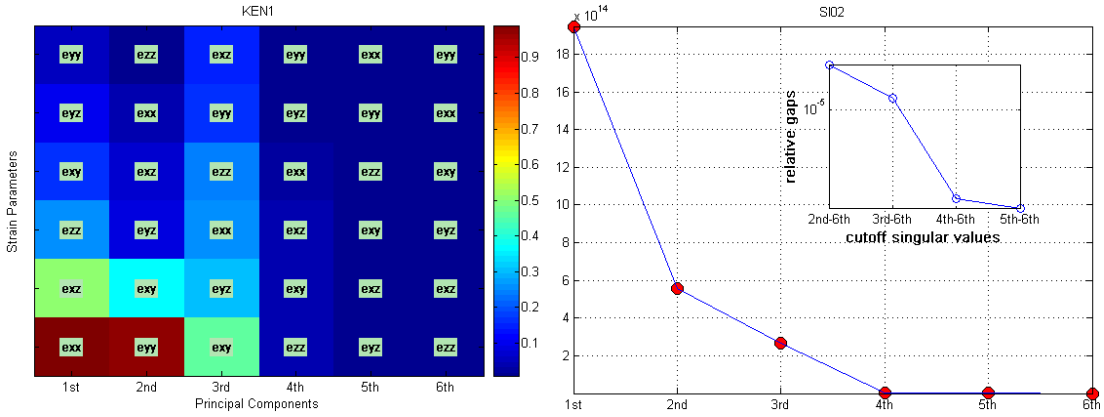

a) b)

Figure 5. Sensitivity analysis results of deformation tensor elements (a) sensitivity analysis of deformation tensor (b) spectral decomposition of the normal matrix.

the singular values asymptotically decay in such a way that the problem is ill-conditioned (see Figure 5b).

Similar to other regularization techniques, replacement of the ill-conditioned problem by a more stable one that is directly related to the main problem, but is less sensitive to perturbation of inputs is preferred. Therefore, matrix A is replaced by A_k which is given by:

$$A_k = U\Sigma_k V^T,\ \Sigma_k = diag(\sigma_1, ..., \sigma_k, 0, ..., 0) \in R^{m\times n},\ k < n \tag{20}$$

A_k approximates A by substituting the last $n-k$ singular values by zero. Through this process the conditioning of the system improves to $k(A_k) = \sigma_1/\sigma_k$ (Aster et al. 2005; Press et al. 1992). The regularized solution is finally given by:

$$x_k = A_k^{-1} b \tag{21}$$

$$A_k^{-1} = V\Sigma_k^{-1}U^T,\ \Sigma_k^{-1} = diag(\sigma_1^{-1}, ..., \sigma_k^{-1}, 0, ..., 0) \tag{22}$$

The central point in any regularization technique is to find a compromise between the resolution of the regularized solution and the stability of the system. This is achieved by finding an optimum regularization parameter. With regard to the TSVD, the number of singular values rejected plays the role of regularization parameter unlike other regularization techniques such as the methods of Tikhonov (1963) and Philips (1962). Perturbation theory of TSVD is well-developed and is the key for finding an optimum regularization parameter in this study. The following theorem within this theory is critical for obtaining an optimum regularization parameter for the TSVD solution (e.g. Hansen 1987).

Theorem 5: For the perturbed TSVD solution $\tilde{x}_k = \tilde{A}_k\tilde{b}$, where $\tilde{A} = A + E = \tilde{U}\tilde{\Sigma}\tilde{V}^T$ and $\tilde{b} = b + e$, assuming that $\|E\| < \sigma_k - \sigma_{k+1}$, the relative error of $\|A_k^{-1}\|$ is bounded by:

$$\frac{\|A_k^{-1} - \tilde{A}_k^{-1}\|}{\|A_k^{-1}\|} \leqslant 3\frac{k_k}{(1-\eta_k)(1-\eta_k-\omega_k)}\frac{\|E\|}{\|A\|} \tag{23}$$

where:

$$\begin{aligned} k_k &= \|A\|\,\|A_k^{-1}\| = \sigma_1/\sigma_k \\ \eta_k &= \|E\|\,\|A_k^{-1}\| = \|E\|/\sigma_k = k_k\|E\|/\|A\| \\ \omega_k &= \|A - A_k\|\,\|A_k^{-1}\| = \sigma_{k+1}/\sigma_k \end{aligned} \tag{24}$$

where k_k is the condition number and ω_k is the size of the relative gap between the spectral values σ_k and σ_{k+1} in spectral representation of A. The proof is given by Hansen (1987).

Theorem 5 shows for $\tilde{A}_k^{-1}$ to be close to A_k^{-1}, the relative gap ω_k should be small. This is because

$$3\frac{k_k}{(1-\eta_k)(1-\eta_k-\omega_k)}\frac{\|E\|}{\|A\|} = 3\frac{\eta_k}{\omega_k}\left[\frac{1}{1-\eta_k-\omega_k} - \frac{1}{1-\eta_k}\right] \tag{25}$$

and therefore, for small ω_k, the term in the square brackets tends to zero. A small ω_k corresponds to a well-determined gap between the singular values σ_k and σ_{k+1}. Therefore, if the SVD is to be successfully truncated at k, then there must be a well-determined gap between the spectral values σ_k and σ_{k+1}.

Considering Theorem 5, to find a tradeoff between the stability and resolution in a regularized TSVD solution in this study, the cumulative relative gaps between each spectral value of the normal matrix and the last (smallest) ones are analyzed. The cumulative relative gaps are plotted against the corresponding pair of spectral

values. The "well determined gap" of Theorem 5 corresponds to the point where a considerable change in the slope of this curve occurs. If a considerable change in the slope of the curve is observed between the spectral values σ_k and σ_p, where σ_p is the smallest nonzero singular value in spectral decomposition of the normal matrix, singular values $\sigma_{k+1}, \ldots, \sigma_p$ are ignored. The cumulative relative gaps for the 3D isoparametric representation of deformation at station KEN1 are shown inset in Figure 5b.

This method appears similar to L-curve analysis, but the methods are different, because in the L-curve analysis technique the norm (or semi-norm) of solution is plotted and analyzed against the norm (or semi-norm) of residuals (Hansen 1992).

3.1.4. *Assessment of Regularization Errors*

How well a regularized solution approximates an exact solution (i.e. the assessment of regularization errors) is an important aspect in any regularization technique. Normally, external information about the sought solution is required. The proposed method within this paper is self-contained, because the assessment of regularization errors does not require any external information about the sought solution and because the horizontal elements of the 3D deformation tensor match the corresponding elements of the 2D deformation tensor. The 2D deformation tensor is obtained from the same approach as the 3D one. However, the assessment of regularization errors on the vertical elements of deformation tensor (e_{xz}, e_{yz}, and e_{zz}) is not a straightforward process. For regularization errors of these parameters only an upper and/or a lower bound limit can be established. This is achieved by comparing the resolution of these elements to resolutions of the 2D elements of deformation.

4. GPS Data, Analysis and Results

The 3D analysis approach outlined in this paper is applied to the GPS network in the Kenai Peninsula in an attempt to analyze the horizontal and vertical pattern of the postseismic uplift in this area. GPS data from seven campaigns (1995, 1996, 1997, 1998.06, 1998.09, 1999 and 2000) were downloaded through the University NAVSTAR Consortium (UNAVCO) Boulder facility. The data were provided by the University of Alaska, Fairbanks and are accessible via download from the Alaska Deformation Array (AKDA) data center.

Requirements for this 3D approach is that GPS stations must be re-measured in at least two successive campaigns. Therefore, a set of 16 stations from the two successive campaigns (1996 and 1998.06) were selected. Ten benchmarks from the leveling survey in 1964 (stations T19D, CROS, K76D, GRAV, DAHL, M78D, S79R, H81D, Z82A and HOMA from Cohen et al. 1995; and Cohen and Freymueller 1997) are included in the selected set of GPS stations. These station locations and the topography of this area are shown in Figure 6.

Three regional permanent stations were also included in this configuration primarily to address the reference frame issue for analyzing the GPS measurements (e.g. Becker et al. 2002). These stations included KEN1 (in the city of Kenai) and KOD1 (on Kodiak Island) from the CORS permanent GPS network and FAIR (in the city of Fairbanks) from IGS network. The locations of these reference stations are shown in the Figures 1 and 6.

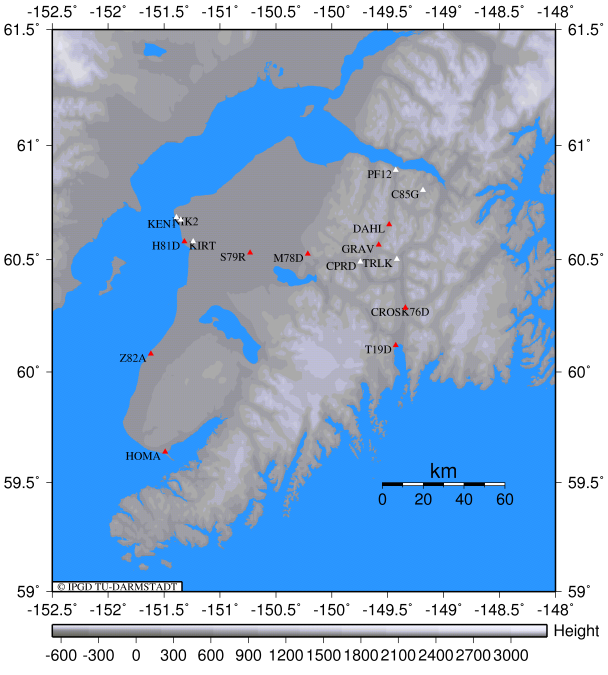

Figure 6. The configuration of the GPS stations in this study. GPS stations are shown by small triangles. GPS stations that are colocated with leveling benchmarks of the survey 1964 are shown in red. Station names are the four character abbreviations used in the processing of the GPS data.

4.1. Analysis

Bernese GPS software Version 4.2 (Beutler et al. 2001) was used to process the data. The IGS (International GNSS Service for Geodynamics) antenna phase center offset and variation calibration table (Rothacher et al. 1995) was used to avoid the systematic effect of using different antenna types in the regional and the local stations. High precision results were obtained by using CODE (Center of Orbit Determination in Europe) precise orbits and earth rotation parameters (Beutler et al. 2001). Minimum elevation cut off angle was set to 10 degrees at all epochs (Rothacher et al. 1998).

The OBS-MAX strategy was used for establishing baselines in both campaigns. Observations whose residuals were larger than 0.003 m were considered outliers and removed from the observation files during the data snooping process. Initial phase ambiguities were resolved using the QIF (Quasi Ionosphere Free) strategy in both campaigns (Mervart 1995). Site-specific troposphere parameters

were estimated every two hours at each station and session.

For long baselines (greater than 10 km) local ionosphere models (Wild 1994; Schaer 1999) that were estimated with the same data set, were used to improve the ambiguity resolution. The consistency of the resolved integer ambiguities with the mathematical models implemented in the processing software was checked by comparing the a posteriori variance of the unit weight in the float solution and that of the fixed solution. A consistent integer ambiguity results in a smooth change in the a posterior variance of unit weight conversely an inconsistent integer ambiguity one can produce abrupt variations in the estimate of this parameter.

As a measure of the precision of the GPS results, RMS repeatabilities of the stations coordinates were studied. Repeatability results clearly showed the poorer quality of the height component when compared to the horizontal components of each station's position. They clearly show that the formal errors for the campaign solutions were too optimistic to be considered. This is due to the fact that systematic and time correlated error sources are neglected in the stochastic model for processing the GPS measurements (Leinen et al. 1999). Therefore, to get realistic accuracy for the GPS results, the formal covariance matrices of the campaign solutions were scaled by a factor of 14.73 for the 1996 campaign and 16.86 for the 1998.06 campaign. Inflation factors were derived from the analysis of the repeatability of the stations coordinates as shown in Figures 7 and 8. Table 1 gives the mean formal errors of the stations coordinates together with their scaled values.

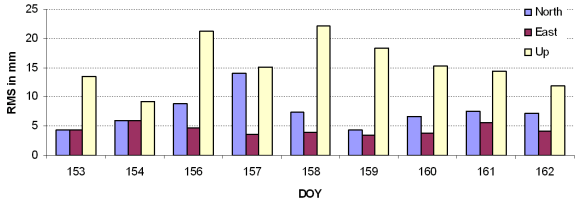

Figure 7. The RMS repeatabilities of the Campaign 1996 for the north, east and up components.

Table 1. Mean formal errors and scaled mean formal errors of the coordinate components of campaigns 1996 and 1998.06.

Campaign	Coordinate Components	Mean Formal Error (mm)	Scaled Mean Formal Error (mm)
1996	Height	0.7526	11.0863
	Latitude	0.3737	05.5044
	Longitude	0.2895	04.2639
1998	Height	0.6526	11.0034
	Latitude	0.3053	05.1467
	Longitude	0.2737	04.6143

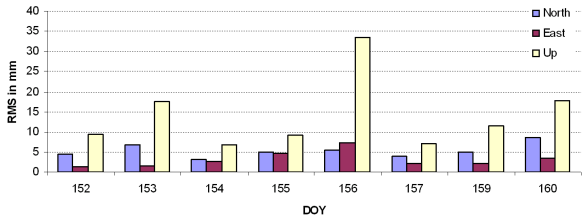

Figure 8. The RMS repeatabilities of the Campaign 1998.06 for the north, east and up components.

4.2. Estimated Velocity Field

Horizontal and vertical velocity fields are computed from the coordinate differences. The computed velocity field together with the associated 95% confidence regions obtained from the propagation of scaled errors are shown in 9 and 10, respectively.

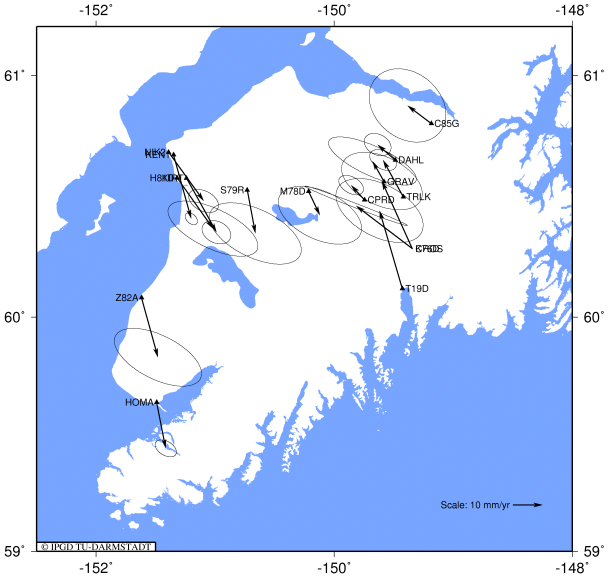

Figure 9. Estimated horizontal velocity field for the deformation network of the Kenai Peninsula.

4.2.1. 3D Pattern of Deformation in Kenai

Since coseismic deformation of the 1964 PWS event extends from Fairbanks in the north to the Kodiak Islands in the south (e.g. Hansen and Eckel 1966) both regional and local stations were incorporated in the computation of the 3D pattern of deformation in this area. First, the 2D pattern of deformation was computed for the study area using the isoparametric approach. To compute the parameters of deformation at each point, a subset of stations (contribution points) was used in the least-squares estimation of

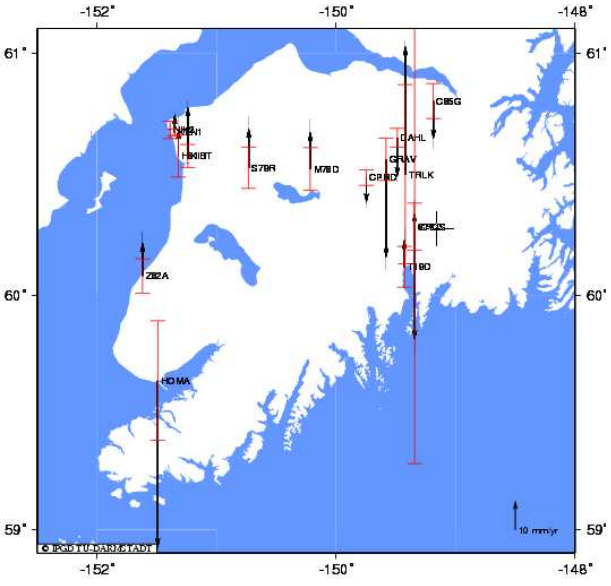

Figure 10. Estimated vertical velocity field for the deformation network of the Kenai Peninsula.

the deformation tensor elements for which the hypothesis test of the a posteriori variance of unit weight is passed. Since station PF12 was removed as an outlier from the final solution of the Campaign 1998.06, it was not included in computations.

The analysis of the discrete Picard condition for all configurations of computation and contribution points proves that the 3D representation of the Earth's surface crustal deformation in the Kenai Peninsula is ill-posed. The topography of the Kenai region also supports this result. The western Kenai area is relatively flat while rugged topography is observed in the east. Consequently, height differences between stations in western Kenai are small when compared to height differences in eastern Kenai. In addition, a set of stations are almost located along a longitudinal line.

Sensitivity analysis of deformation tensors shows that the vertical parameters of deformation are more sensitive to perturbations of inputs. Therefore, depending on the number of singular values to be rejected these parameters will loose more resolution than the other parameters in regularized deformation tensors.

The optimum number of singular values to be rejected was obtained using the method in Section 3.1.3 of this paper. Regularized deformation tensors were then computed in the geocentric Cartesian coordinate system. Computed deformation tensors were then transformed to the spherical coordinate system. Spherical approximation of the principal strains (e_I, e_{II}, e_{III}) and their orientation with respect to the curvilinear coordinate axes of the Spherical coordinate system are computed by eigenvalue-eigenvector decomposition of the transformed deformation tensors. The accuracy of random eigenspectra was first given by Agelier at al. (1982), and later independently derived by Soler and van Gelder (1991) and further extended to second order approximation by Xu and Grafarend (1996), Xu (1999) and Han (2010). In this study, computation of the variance-covariance matrices of principal strains is based on Soler and van Gelder (1991).

To visualize the horizontal pattern of deformation, the cross section of the deformation quadratic (expressed in the spherical coordinate system) and the horizontal spherical coordinate system is set up. This quadratic polynomial is then transformed to its principal axes. The horizontal principal strains and their orientation in the spherical coordinate system are the corresponding eigenvalues and eigenvectors of this transformation. To illustrate the vertical deformations, principal strain parameters in the third dimension (vertical component) are interpolated using a biharmonic spline interpolation technique (Sandwell 1987). Figure 11 illustrates the 3D pattern of deformations.

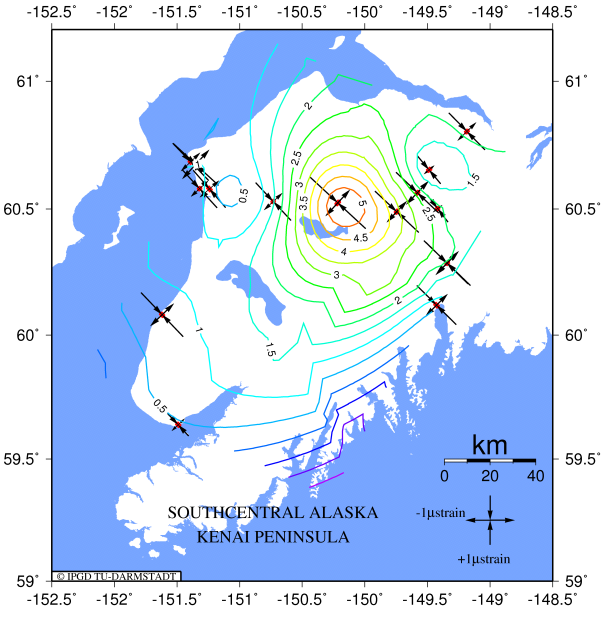

Figure 11. 3D Isoparametric representation of deformations in the Kenai Peninsula.

In the two-dimensional approach to the analysis of deformation, the projection of vector lengths onto the surface of the horizontal reference datum accounts for the effect of vertical deformations on the horizontal elements of deformation tensor. For the centimeter-level vertical deformations in this area, the effect of vertical deformations on the horizontal parameters of strain is ignored. Therefore, first-order differences are the result of the regularization error in the 3D horizontal parameters of strain. The statistical significance of these differences, as well as the redundancy of observation in estimating both the two- and three-dimensional deformation tensors should be carefully taken into consideration. To see if the differences mentioned above are stochastically signif-

icant their confidence intervals were computed. Table 2 provides the numerical details. In this table parameters $|\Delta e_I|$ and $|\Delta e_{II}|$ are the differences of the corresponding horizontal principal strains obtained from the 2D and 3D analysis approaches. σ_I and σ_{II} are the corresponding confidence intervals of these parameters that were derived by error propagation using the errors of the 2D and 3D horizontal principal strains.

Table 2. Regularization errors in the 3D horizontal principal strains of the isoparametric representation of deformation versus the corresponding confidence intervals.

Station	3D Isoparametric			
	$\|\Delta e_I\|$	σ_I	$\|\Delta e_{II}\|$	σ_{II}
KEN1	0.1580	0.1295	0.1460	0.2030
C85G	0.2540	0.2572	0.4490	0.3556
CPRD	0.0920	0.2106	0.2590	0.1773
CROS	0.1220	0.2482	0.1650	0.2379
DAHL	0.1740	0.1931	0.2750	0.1849
GRAV	0.2410	0.2945	0.3820	0.3750
H81D	0.1530	0.3687	0.1490	0.4319
HOMA	0.0360	0.1812	0.0420	0.4220
K76D	0.1450	0.2893	0.2180	0.2958
KIRT	0.0420	0.2208	0.0350	0.3159
M78D	0.0250	0.3940	0.2480	0.4582
NIK2	0.1260	0.1791	0.1240	0.2158
S79R	0.0370	0.4074	0.0170	0.4737
T19D	0.0050	0.2469	0.0060	0.2712
TRLK	0.0150	0.1673	0.0250	0.1796
Z82A	0.0170	0.3611	0.0170	0.6583

Table 2 shows the differences of the horizontal principal strains of the 3D Isoparametric and the 2D Isoparametric approaches are stochastically meaningful for stations KEN1, DAHL and C85G. Since the redundancies of observations for estimating the 2D and 3D isoparametric deformation tensor at these stations are small (Hossainali, 2006), it is not possible to assign the abovementioned differences only to regularization errors. The results of the sensitivity analysis of the deformation tensor show that for the GPS network of this study the vertical parameters of deformation are more sensitive to perturbations of inputs. Smaller resolution of these parameters in the corresponding resolution matrices of both approaches also supports this argument. Therefore, regularization errors of the vertical elements of the deformation tensor are larger than the horizontal ones. Nevertheless, the poor redundancy of observations in the GPS network in this study makes the assessment of the regularization error of the vertical parameters of deformation impossible. Based on regularization errors of the horizontal parameters of deformation and comparing the resolutions of the vertical and horizontal parameters, estimating an upper bound or a lower bound limit for the regularization error of the vertical parameters of deformation would have been possible. The obtained features in vertical deformation in this study confirm the independent results of the other studies. That show regularization errors do not dominate the results of the vertical deformations of this study.

The computed pattern of vertical deformation is in a good agreement with Cohen and Freymueller (1997) (Figure 2). Both are consistent with the trend of tectonic features including the Alaska Aleutian trench, the orientation of major terranes, the strike of the Border Range Fault, the orientation of Cook Inlet and the strike of the Alaska range volcanoes to the west. Cohen and Freymueller (1997) acknowledged that not all parts of their pattern are well constrained by the data but they suggest that the dome pattern of uplift trending SW to NE and the location of maximum uplift were robust. These deformation features are also visible in the computed pattern of vertical deformation in this study.

5. Conclusions

The 3D pattern of deformation obtained for the Kenai Peninsula represents an inhomogeneous deformation field. Estimated horizontal and vertical velocity fields confirm the spatial pattern of variability in the deformation of this area. Inhomogeneity of deformation is a characteristic feature of many deformation fields. The degree of the misfit of the functional models in 3D isoparametric and 3D Lagrangian representations of deformation is also a function of the inhomogeneity of the deformation.

The nature of the inhomogeneity of the deformation may change from one area to another. When no a priori information is available for setting up an advanced mathematical model the analysis of inhomogeneous deformation fields is likely confined to the application of the mathematical models that are tailored to homogeneous deformation. The conditioning of the problem will worsen when an inhomogeneous deformation field is analyzed. According to Corollary 2, the conditioning of the problem is proportional to the power of two of the condition number of the system of simultaneous equations.

The adequacy of the functional models in the 3D Isoparametric and Lagrangian representations of deformation for analyzing a deformation is assured through the Global Model Test. Using the Global Model Test, the list of contribution points is determined when the parameters of deformation are calculated at a computation point. Realistic analysis of regularization errors requires adequate observational redundancy. The observational redundancy is controlled by the number of contribution points to be used for estimating the parameters of deformation at a certain point of a deformable body. Therefore, in complex deformation fields increasing the density of the network can assist the better assessment of regularization errors. The GPS network in Kenai is too sparse. Nevertheless, the conformance of the obtained pattern of deformation to the previously obtained results proves that estimated parameters of deformation are not dominated by regularization errors.

Acknowledgments

The GPS data from the Kenai Peninsula were obtained from UNAVCO (University NAVSTAR Consortium) Boulder facility to this study. The Geodesy Lab at the University of Alaska had provided the data to UNAVCO. Hereby, their cooperation as well as the corresponding sponsors is appreciated. The fault trace coordinates in South-Central Alaska was also provided by the Geodesy Lab at the University of Alaska. Their cooperation in this respect is also appreciable. We are also thankful to Dr. Yüksel Altiner from BKG (Bundesamt für Kartographie und Geodäsie) for the programs he kindly provided us for checking the programs which were written for the 2D analysis of deformation. Source of the developed computer codes are available to interested readers via the Institute of Physical Geodesy, TU-Darmstadt.

References

Altiner Y., 1999, Analytical Surface Deformation Theory for Detection of the Earth's Crust Movements, Springer.

Aster R.C., Borchers B., et al., 2005, Parameter Estimation and Inverse Problems, Elsevier Academic Press.

Becker M., Bruyninx C., et al., 2002, Processing and Submission Guidelines for GPS Solutions to be Integrated to a WEGENER Data Base. Proceedings of WEGENER 2002, Jun 12-14, NTUA Athen.

Berber M., Dare P.J., et al., 2003, On the application of robustness analysis to geodetic networks. Annual Conference of the Canadian Society for Civil Engineering.

Beutler G., Bock H., et al., 2001, Bernese GPS software version 4.2, Astronomical Institute of Bern.

Bibby H.M., 1982, "Unbiased estimate of strain from triangulation data using the method of simultaneous reduction." Tectonophysics 82:161-174.

Brown L.D., Reilinger R.E., et al., 1977, "Post- seismic crustal uplift near Anchorage, Alaska." J. Geophys. Res. 82:3369-3378.

Brunner F.K., 1979, "On the analysis of geodetic networks for the determination of the incremental strain tensor." Survey Review XXV 192:56-67.

Chen R., 1991, On the horizontal crustal deformations in Finland. Helsinki, Finish Geodetic Institute.

Cohen S.C. and Freymueller J.T., 1997, "Deformation on the Kenai Peninsula, Alaska." J. Geophys. Res. 102:20,479-20,487.

Cohen S.C., Holdahl S., et al., 1995, "Uplift of the Kenai Peninsula Alaska since the 1964 Prince William Sound Earthquake." J. Geophys. Res. 100:2031-2038.

Crosilla F., 2003, Procrustes Analysis and Geodetic Science. Geodesy The Challenge of the 3rd Millennium. W. Friedrich, Krumm, Volker and S. Schwarze, Springer Verlag, 287-292.

Dermanis A., 1981, "Geodetic estimability of crustal deformation parameters." Quaterniones Geod. 2:159-169.

Dermanis A., 1985, "The role of frame definitions in the geodetic determination of crustal deformation parameters." Bull., Geod., 59:247-274.

Dermanis A. and Grafarend E., 1981, "Estimability analysis of geodetic, astronomic and geodynamical quantities in very long baseline interferometry." Geophys. J. R. Astr. Soc., 64:31-64.

Dermanis A. and Grafarend E.W., 1992, The finite element approach to geodetic computation of two- and three-dimensional deformation parameters: A study of frame invariance and parameter estimability. Cartography-Geodesy, Maracaibo/Venezuela, Institute de Astronomia y Geodesia, Madrid.

Dief A., 1986, Sensitivity analysis in linear systems, Springer.

Dryden, I. L. and K. V. Mardia (2002). Statistical Shape Analysis, John Wiley & Sons.

Flügge W., 1972, Tensor analysis and continuum mechanics, Springer.

Frank F.C., 1966, " Deduction of earth strains from survey data." Bull. Seismol. Soc. Am. 56:35-42.

Gutenberg B. and Richter C.F., 1949, Seismicity of the earth and associated phenomena, Princeton Univ. Press.

Hansen P.C., 1990, "The Discrete Picard Condition for Discrete Ill-Posed Problems." BIT 30:658-672.

Hansen P.C., 1992, "Analysis of Discrete Ill-Posed Problems by Means of the L-Curve." SIAM Review 34(4):561-580.

Hansen P.V., 1987, "The Truncated SVD as a Method for Regularization." BIT 27:534-553.

Hansen W.R. and Eckel E.B., 1966, A summary description of the Alaska earthquake- its setting and effects. The Alaska earthquake of March 27, 1964: Field investigations and reconstruction efforts.

E. Hansen, and others, US Geological Survey Prof. Paper 541:1-37.

Hanson R.J., 1971, "A Numerical Method for Solving Fredholm Integral Equations of the First Kind Using Singular Vlaues." SIAM Journal on Numerical Analysis 8(3):616-622.

Han J.Y., 2010, Non-iterative approach for solving the indirect problems of linear reference frame transformations, J. Surv. Eng., ASCE, 136(4):150-156, DOI:10.1061/(ASCE)SU.1943-5428.0000026.

Higham N.J., 2002, Accuracy and stability of numerical algorithms. Philadelphia, SIAM.

Holdahl S.R. and Sauber J., 1994, "Coseismic slip in the 1964 Prince William Sound earthquake: A new geodetic inversion." Pure Appl. Geophys. 142:55-82.

Hossainali M.M., 2006, A Comprehensive Approach to the Analysis of the 3D Kinemaics of Deformation. Institute of Physical Geodesy. Darmstadt, Darmstadt University of Technology: 152, PhD Thesis.

Jaeger J.C., 1969, Elasticity Fracture and Flow with Engineering and Geological Applications, Methuen & Co. LTD.

Jain M.K., Iyengar S.R.K., et al., 2003, Numerical methods for scientific and engineering computation, New Age International (P) Limited, Publishers.

Johnson R.A. and Wichern D.W., 2002, Applied multivariate statistical analysis, Prentice Hall, Upper Saddle River.

Kanamori H., 1997, "The energy release in great earthquakes." J. Geophys. Res. 82:2981-2987.

Krumm F. and Grafarend E., 2002, "Datum-free Deformation Analysis of ITRF networks." Artificial Satellites 37:75-84.

Lambeck K., 1988, Geophysical Geodesy: The Slow Deformation of the Earth, Clarendon Press: Oxford.

Leinen S., Groten E., et al., 1999, Deformation monitoring of Karasu Viaduct with GPS and levelling. Proceeding of the third Turkish-German joint geodetic days, Istanbul, Istanbul.

Lichtenegger H. and Sünkel H., 1989, "Mathematische-Geophysikalische Model, in Österreichische Beträge zum Wegener-Medals-Projekt, Mitteilungen der geodätischen Institute der Technischen Universität Graz." 65:61-80.

Love A.E.H., 1944, A treatise on the mathematical theory of elasticity, Dover publications.

Mervart L., 1995, Ambiguity resolution techniques in Geodetic and Geodynamic applications of Global Positioning System. Astronomical Institute. Bern, University of Bern. Ph.D.

Parkin E., 1972, Horizontal crustal movements, in The Great Alaska Earthquake of 1964. Washington D.C., National Academy of Sciences.

Philips D.L., 1962, "A technique for the numerical solution of certain integral equations of the first kind." J. ACM 9:84-97.

Plafker G., 1971, "Tectonics, in The Great Alaska Earthquake of 1964." Geology, National Academy of Sciences, Washington, D.C.: 47-122.

Press H.W., Flannery B.P., et al., 1992, Numerical Recipes in FORTRAN Example Book: The Art of Scientific Computing, Cambridge University Press.

Rothacher M., Gurtner W., et al., 1995, Azimuth and elevation¬dependent phase center corrections for geodetic gps antennas estimated from GPS Calibration campaigns. Paper presented at the XXI General Assembly of IUGG, Boulder, Colorado.

Rothacher M., Springer T.A., et al., Eds., 1998, Processing strategies for regional GPS Networks. Advances in Positioning and Reference Frames, Int. Assoc. of Geodesy Symposia, Berlin Heidelberg, p. 93-100.

Sandwell D.T., 1987, "Biharmonic spline interpolation of GEOS-3 and SEASAT altimeter data." Geophys. Res. Let. 14:139-142.

Savage J.C. and Plafker G., 1991, "Tide gauge measurements of uplift along the south coast of Alaska." J. Geophys. Res. 96:4325-4335.

Schaer S., Beutler G. et al., 1999, The Impact of Atmospheric and Other Systematic Errors on Permanent GPS Networks. paper presented at IAG Symposium on Positioning, July 21, Birmingham, UK.

Segall P., and Matthews M.V., 1988, "Displacement calculations from geodetic data and the testing of geophysical deformation models." J. Geophys. Res. 93:14954-14966.

Sokolnikoff I.S., 1956, Mathematical Theory of Elasticity, McGraw-Hill Book Company Inc.

Soler T., Boudewijn H. et al., 1991, "On covariances of eigenvalues and eigenvectors of second-rank symmetric tensors." Geophys. J. Int. 105:537-546.

Stacy F.D., 1977, Physics of The Earth, John Wiley and Sons.

Terada T. and Miyabe N., 1929, "Deformation of the Earth Crust in Kwansai District and its Relation to the Orographic Features." Bull. Earthquake Res. Ins. U. of Tokyo 7, Part 2.: 223-241.

Tikhonov A.N., 1963, "Solution of incorrectly formulated problems and the regularization method." Soviet Math. Dokl 4: 1035-1038.

Tikhonov A.N. and Arsenin V.Y., 1977, Solutions of Ill-Posed Problems. Washington, D.C., V. H. Winston & Sons.

Varah J.M., 1973, "On the Numerical Solution of Ill-Conditioned Linear Systems with Applications to Ill-Posed Problems." SIAM Journal on Numerical Analysis 10(2):257-267.

Watkins D.S., 2002, Fundamentals of Matrix Computations, John Wiley & Sons.

Welsch W., 1979, "A review of the adjustment of free networks." Surv. Rev. 194(25):167-180.

Wild U., 1994, Ionosphere and Ambiguity Resolution. Proceedings of the 1993 IGS Workshop, University of Berne.

Wittenburg R., 2003, Geodetic description of 3D body deformation. Geodesy The Challenge of the 3rd Millennium. F. W. Krumm and V. S. Schwarze, Springer Verlag: 401-404.

Xu P., 1994, "Testability and adjustment in free net models." J. Geod. Soc. Japan Supplement issue: 315-320.

Xu P., 1995, "Testing the hypotheses of non-estimable functions in free net adjustment models." Manuscripta Geodetica 20:73-81.

Xu P., 1997, "A general solution in geodetic nonlinear rank-defect models." Bollettino di Geodesia e Scienze Affini 1:1-25.

Xu P.L., 1998, Truncated SVD Methods for Linear Discrete Ill-posed Problems, Geophys. J. Int., 135, 505-514.

Xu P., Shimada S., Fujii Y., Tanaka T., 2000, "Invariant geodynamic information in geometric geodetic measurements." Geophys. J. Int. 142:586-602.